Rodents and satellites: Predicting mice abundance and distribution with Sentinel-2 data

Verónica Andreo[a,b,c,*], Mariana Belgiu[a], Diana Brito Hoyos[d], Frank Osei[a], Cecilia Provensal[d], Alfred Stein[a]

[a] *Department of Earth Observation Sciences, Faculty of Geo-Information Science and Earth Observation, University of Twente, Hengelosestraat 99, 7514 AE, Enschede, The Netherlands*
[b] *Consejo Nacional de Investigaciones Científicas y Técnicas (CONICET), Buenos Aires, Argentina*
[c] *Instituto Nacional de Medicina Tropical, Neuquén y Jujuy s/n. 3370, Puerto Iguazú, Misiones, Argentina*
[d] *Departamento de Ciencias Naturales, Facultad de Ciencias Exactas, Físico-Químicas y Naturales, Universidad Nacional de Río Cuarto, Ruta 36 – Km 601. 5800 Río Cuarto, Córdoba, Argentina*

ARTICLE INFO

ABSTRACT

Remote sensing data is widely used in numerous ecological applications. The Sentinel-2 satellites (S2 A and B), recently launched by the European Spatial Agency's (ESA), provide at present the best revisit time, spatial and spectral resolution among the freely available remote sensing optical data. In this study, we explored the potential of S2 enhanced spectral and spatial resolution to explain and predict mice abundances and distribution in border habitats of agroecosystems. We compared the predictive ability of different vegetation and water indices derived from S2 and Landsat 8 (L8) imagery. Our analyses revealed that the best predictor of mice abundance was L8-derived Enhanced Vegetation Index (EVI). S2-based indices, however, outperformed those computed from L8 bands for indices estimated simultaneously to mice trappings and for mice distribution models. Furthermore, indices including S2 red-edge bands were the best predictors of the distribution of the two most common rodent species in the ensemble. The findings of this study can be used as guidelines when selecting the sensors and vegetation variables to be included in more complex models aimed at predicting the distribution and risk of various vector-borne diseases, and especially rodents in other agricultural landscapes.

1. Introduction

Remote sensing data is nowadays widely used in environmental and ecological studies and applications including the field of disease ecology or landscape epidemiology (Carroll et al., 2009). Data acquired by different satellite sensors like Landsat TM and ETM+ (Malahlela et al., 2018), NOAA's AVHRR, SPOT (Beck et al., 2000; Glass et al., 2002; Ostfeld et al., 2005) or MODIS (Andreo et al., 2011; Andreo et al., 2014; Midekisa et al., 2014; Neteler et al., 2011), among others, were used for mapping animal host or vector habitats and predicting human transmission risk at different spatial and temporal scales. Currently, the availability of the new generation of medium resolution sensors, such as the Multi-Spectral Instrument (MSI) on board the Sentinel-2 (S2) satellites from the European Spatial Agency (ESA), offers new opportunities for many ecological applications. S2 MSI main features include increased revisit frequency (5 days since 7 March 2017 with the launch

of S2B), finer spatial resolution (10 m resolution for visible and near-infrared (NIR) bands) and increased spectral resolution (13 bands including coastal aerosol band, 3 red-edge bands, water vapour, short wave infrared (SWIR)-cirrus and two additional SWIR bands). Importantly, the data from this satellite are completely free of charge. The use of these new data is in steep increase in various research and application fields. Several studies have investigated the application of S2 imagery, for example in mapping and monitoring burnt areas (Verhegghen et al., 2016), crop types and invasive species, in evaluating water constituents (Dörnhöfer et al., 2016) or in coral bleach detection (Hedley et al., 2012). However, to the best of our knowledge, there are just a few applications of S2 data for animal and disease ecology (Peckham and Sinha, 2017).

Rodents are among the most studied animals mainly because they are hosts or reservoirs of several different viruses known to cause severe and even fatal diseases in humans all over the world. The most severe

---

Fig. 1. Spatial distribution of rodent traplines in the rural area of Chucul (Córdoba province, Argentina). Period 2016–2017.

rodent-borne viruses are those causing hemorrhagic fevers: the arenaviruses (e.g.: Junin virus, causal agent of the Argentine Haemorrhagic Fever) and the hantaviruses (e.g.: Sin Nombre and Andes viruses, causal agents of Hantavirus Pulmonary Syndrome in the Americas; Hantaan, Puumala and Seoul viruses, causal agents of the Hemorrhagic Fever with Renal Syndrome in Europe and Asia, among others). In general, each virus is associated with a single rodent species in which it establishes a prolonged infection (only very rarely it produces disease in the animal host). These viruses are transmitted to humans predominantly via airborne particles of saliva, urine or faeces from infected rodents (Meerburg et al., 2009; Watson et al., 2014). In this context, the relationship among the host-vector abundance and variables of its habitat, i.e., which habitat variables and values of habitat variables determine the presence and abundance of hosts and vectors in space and time, becomes crucial (Mills and Childs, 1998). Therefore, the monitoring of habitats and the study of relevant environmental variables (at a proper spatial and temporal resolution) by means of remote sensing is valuable knowledge that can be integrated and applied in the development of predictive models (Mills and Childs, 1998) and operative systems for risk monitoring and early warning (Porcasi et al., 2012).

The agroecosystems of central Argentina are inhabited by several rodent species that can be the hosts to different viruses: *Calomys musculinus* (corn mouse) is the natural reservoir of Junín arenavirus, the etiological agent of the Argentine Hemorrhagic Fever (AHF) (Sabattini et al., 1970); *Akodon azarae* (Pampean grassland mouse) is the reservoir of the hantavirus Pergamino (Levis et al., 1998); *Calomys venustus* (Córdoba vesper mouse) is the reservoir of the arenavirus Latino-like (Calderón et al., n.d.) and *Oligoryzomys flavescens* (yellow pygmy rice rat) is the host of the virus Lechiguanas and Hu39694 known to cause Hantavirus Pulmonary Syndrome in humans (Levis et al., 1998). Previous studies in such agroecosystems (Andreo et al., 2009a, b; Andreo et al., 2009b; Polop et al., 2008; Polop et al., 2012; Simone et al., 2012)

have used low to middle resolution satellite imagery (NOAA-AVHRR, MODIS, Landsat TM and ETM +) to relate habitat features derived from remote sensing (esp. traditional vegetation indices like NDVI) with mice abundances. The reported results have been clear for one particular rodent species in long-term studies, namely *A. azarae* in railroad banks, but not so clear for other rodent species in crop field borders (Andreo et al., 2009a; Andreo et al., 2009b; Simone et al., 2012). This might be related to a poor delineation and consequently, a poor characterization of their habitats, i.e., crop field borders, given the spatial resolution of remote sensing data used. An increased spatial resolution (10 m in S2 vs 30 m in L8) is therefore expected to reap benefits in the prediction of mice abundance and distribution. Moreover, vegetation indices based on S2 red-edge bands, that have proven to be related to vegetation phenology and health status (Immitzer et al., 2016), are expected to have higher predictive power since they can better relate to mice habitat quality.

The aim of this study was to explore the potential advantages of using S2 data and compare to L8 in their ability to explain and predict mice abundance and distribution in linear habitats of agroecosystems from central Argentina.

2. Materials and methods

2.1. Study area

The study was carried out in the south-west of Córdoba province, Argentina (Fig. 1). The area is a typical undulating pampean plain (600–900 m a.s.l.). The climate is temperate with an average temperature of 23 °C in January and 6 °C in July. Annual mean rainfall is about 800–900 mm, mostly concentrated in summer months. The natural transitional landscape of woodland (dominated by *Prosopis alba*, *P. nigra*, *P. caldenia*, *Celtis tala*, *Acacia caven* and *Geoffroea decorticans*) and

pampean natural grassland (*Stipa spp.*) remains in patches among crop fields. The vegetation has undergone marked alterations as a result of agriculture and cattle farming. Currently, the landscape mainly consists of individual crop fields surrounded by wire fences with borders dominated by weed species. In general, these border habitats are less disturbed than agricultural fields, maintaining relatively high plant cover throughout the year, thus providing good habitat conditions for small rodent species (Bilenca and Kravetz, 1998; Ellis et al., 1997). *A. azarae*, *C. musculinus* and *C. venustus* are the most abundant species inhabiting such border habitats (Andreo et al., 2009a; Simone et al., 2012). However, these species show temporal and spatial variations in their abundance. *A. azarae* and *C. venustus* are usually found in relatively stable habitats with high vegetation cover, while *C. musculinus* has been also captured in crop fields (Busch et al., 2000). *O. flavescens* is found in border habitats, though usually in much lower numbers (Mills et al., 1991).

2.2. Small rodents data

We used mark-recapture data from mice live-trapping conducted on four consecutive nights on a seasonal basis: November 2016 (spring), February 2017 (summer) and April 2017 (autumn), in 24 traplines located in crop-field borders that were selected from satellite images as described in (Simone et al., 2010). Each trapline consisted of 20 Sherman-type live traps baited with a mixture of peanut butter and cow fat, placed ≈ 5 m apart from each other. For summer and autumn 2017, 11 additional borders were selected according to neighbouring crops (i.e. maize or soybean). Population abundance was estimated from the minimum number of animals known to be alive (MNKA). The spatial distribution of traplines is shown in Fig. 1.

2.3. Remote sensing data

We downloaded 11 S2 scenes and 11 L8 scenes (path 229, row 83) for the period September 2016–April 2017 (Table 1). Top of atmosphere (TOA) Level-1C S2 scenes were processed to Bottom of atmosphere (BOA) reflectance (Level-2A surface reflectance product) using sen2cor plugin v2.3.1 (Muller-Wilm et al., 2013) available on the Sentinel Application Platform (SNAP) distributed under GNU GPL license.

L8 imagery was obtained as surface reflectance products (BOA) directly from United States Geological Service (USGS) site (https://earthexplorer.usgs.gov/). All images were imported into (GRASS GIS Development Team, 2018) database and co-registered to a single scene, with overall mean RMSE < 5 m (Table 1). S2 bands 5, 6, 7, 8A, 11 and 12 were resampled to 10 m by nearest neighbour resampling (Ng et al., 2017; Zheng et al., 2017) and further used to estimate

Table 1
Date of S2 and L8 images used and root mean squared error (RMSE) corresponding to the co-registration of images. The unit of RMSE is meters (m).

Landsat-8		Sentinel-2	
Date	RMSE	Date	RMSE
2016/10/01	1.90	2016/09/02	5.02
2016/11/02	8.60	2016/09/22	3.60
2016/11/18	1.07	2016/10/02	7.08
2016/12/04	3.00	2016/11/01	4.20
2016/12/20	6.00	2016/11/11	8.80
2017/01/05	0.90	2016/12/01	3.06
2017/01/21	6.50	2016/12/11	3.03
2017/02/06	0.50	2017/01/30	5.70
2017/02/22	2.40	2017/02/19	0.03
2017/03/10	2.30	2017/03/21	2.60
2017/04/11	5.03	2017/04/30	7.80
Mean RMSE	3.48	Mean RMSE	4.62

different vegetation and water indices (see Table 6 in Section 5, Appendix).

We extracted spatially aggregated average values for each index in the pixels that were overlapped by the traplines. Fig. 2 shows an example of the resultant polygons for S2 and L8 images. All remote sensing processing was done in (GRASS GIS 7 Development Team, 2018).

2.4. Statistical analysis

We fitted univariate generalized semi-parametric models (Green and Yandell, 1985) between mice counts and each S2 and L8-derived vegetation and water index. We treated the observed number of mice y_{ij} at sampling locations $i = 1, \ldots, n$ and seasons $j = 1,2,3$ as Poisson random variables with mean μ_{ij}, and linked with a linear predictor $log(\mu_{ij}) = \alpha_j + f(x) + U_i + V_i$. Here, α_j are random intercepts across seasons, $f(x)$ is a nonlinear smooth function of the vegetation and water indices, and the U_i and V_i denote correlated and uncorrelated spatial variation across sampling locations, respectively. The correlated and uncorrelated spatial variation parameters account for extra Poisson variation due to important unmeasured explanatory variables.

We used quadratic penalized splines with truncated power basis functions for $f(x)$, leading to the following parametrization

$$log(\mu_{ij}) = \alpha_j + \beta_1 x_i + \beta_2 x_i^2 + \sum_{m=1}^{M} \gamma_m (x_i - \kappa_m)^2 + U_i + V_i \quad (1)$$

where β_1 and β_2 are fixed effect coefficients, $\gamma_1, \ldots, \gamma_M$ are the coefficients of the quadratic spline basis $(x_i - \kappa_m)^2$ with knots $\kappa_1, \ldots, \kappa_M$. We applied a Bayesian model fitting, hence all parameters were assumed unknown and were assigned an a priori distributions.

For α_j, we set $\alpha_1 = 0$ for identification purposes and assumed non-informative prior knowledge with a flat distribution for α_2 and α_3. For the fixed effect coefficients β_1 and β_2, we assumed a non-informative Gaussian prior distribution with zero mean and a precision of 0.001. For the random effect coefficients, $\gamma_1, \ldots, \gamma_n$, Gaussian prior distributions with zero mean and gamma precision $\theta_\gamma \sim Ga(0.05,0.05)$ were assumed. Similarly, we assigned a Gaussian prior distribution with zero mean and gamma precision $\theta_U \sim Ga(0.05,0.05)$ to the uncorrelated spatial variation U_i. For the spatially correlated variation, we assigned a zero mean multivariate Gaussian process $V_i \sim MVN(0, \Sigma)$ with variance-covariance matrix $\Sigma = exp(-\phi d)$ defined by an isotropic exponential function based on the distance between observation pairs d and the rate of distance decay parameter ϕ. We assigned a uniform prior distribution to the distance decay parameter $\phi \sim unif(0,6000)$. The prior distributions together with the likelihood of the data were updated to obtain the posterior distributions of the parameters by drawing 10,000 Markov Chain Monte Carlo (MCMC) simulations of the Gibbs sampler with a thinning of 1, of which the first 2000 were discarded.

We also ran univariate generalized semi-parametric models for the two most common species of the ensemble: *A. azarae* and *C. musculinus*. Since count data contained many zeroes, we converted abundances into presence-absence data and ran logistic type models following the same approach described above.

The models were implemented in the WINBUGS 1.4.3 software package (Spiegelhalter, 2008). Convergence was assessed graphically using autocorrelation plots of the traces. We used the posterior predictive probabilities, as suggested by (Lunn et al., 2012), to assess the adequacy of the models. We generated posterior predictive distributions under each model and compared them with the observed data. We then calculated Bayesian *p*-values which give the predictive probability of obtaining an extreme result. A *p*-value close to 0 or 1 suggests that the generated data are extreme and hence the fit is poor, whereas a *p*-value close to 0.5 suggests that the generated data are compatible with the model. The deviance information criterion (DIC) (Spiegelhalter et al., 2002) was used to assess the relative goodness-of-fit of the different univariate models. Models with lower DIC value were judged to
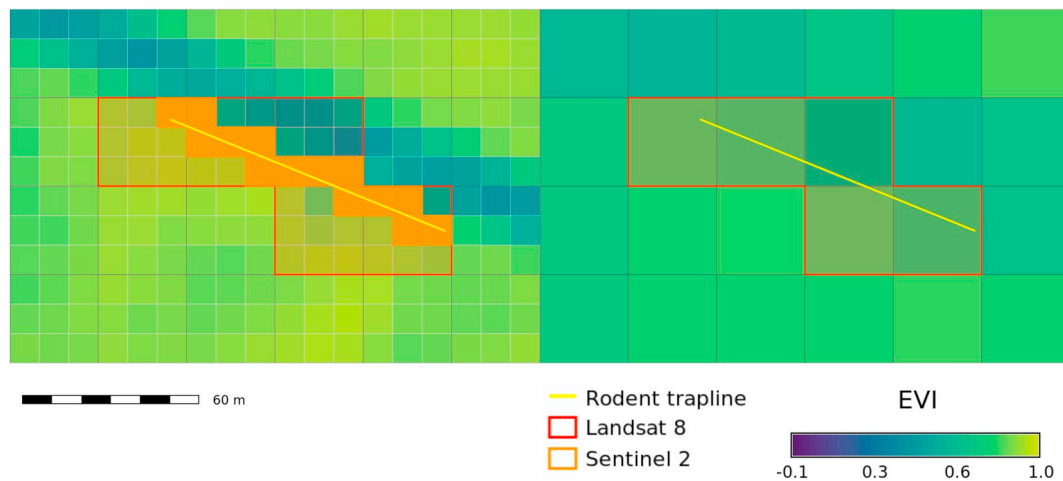
Fig. 2. Comparison of pixel sizes and corresponding EVI values in Sentinel-2 and Landsat-8 scenes. The figure shows how S2 imagery identifies and "sees" the road, while L8 data misses it.

be the best representation of the data. We addressed the ability of models to predict total mice abundances (all species together) and *A. azarae* and *C. musculinus* distribution using the satellite derived indices obtained simultaneously to the mice trapping (t_0), and 1 and 2 months before the trappings ($t - 1$ and $t - 2$, respectively). We performed different comparisons: first we assessed all satellite indices together, both for total mice counts and *A. azarae* and *C. musculinus'* distribution. Then, to assess the effects of different spatial resolution in the predictive ability of satellite indices, we compared models including indices that are common to both S2 and L8. Finally, we evaluated the performance of satellite indices that are exclusive to S2, i.e., those using the red-edge and narrow NIR bands that are absent in the L8 sensor.

3. Results

A total of 464 individuals were captured during the three trapping seasons (from spring 2016 to autumn 2017) with a sampling effort of 7520 trap-nights (estimated as traps * nights). *C. musculinus* was the most common species (39%), followed by *A. azarae* (32%), *C. venustus* (22%) and *O. flavescens* (4%). Fig. 3 shows the abundances of rodent species per trapline over the three sampling seasons.

We obtained adequate fit for all models as their average Bayesian *p*-values, i.e., the predictive probability of obtaining an extreme result, were within the acceptable range and close to 0.5 (Fig. 4a). Fig. 4b shows the relative seasonal effects of the second and third trapping seasons (summer and autumn) compared with the first trapping season (spring, reference season). In all instances, the effects of the second and third trapping seasons were higher than the first, except for model #51 testing Simple Ratio, SR, from L8 in $t - 1$ as mice abundance predictor. The second trapping season (summer) had a higher effect than the third trapping season from model 1 up to model 20 (all S2 indices estimated at t_0). Moreover, the proportion of spatial correlation to the overall spatial variation ranged from 48 to 51% (see Fig. 4c), suggesting nearly equal variances for the correlated and uncorrelated (random) spatial variation. Similar results were obtained for the distribution models fitted for *A. azarae* and *C. musculinus* (see Figs. 1 to 3 in Supplementary Material).

Table 2 shows the first 10 univariate models for mice total counts sorted according to increasing DIC values. The best predictor of mice total counts in the period spring 2016 – autumn 2017 was the Enhanced Vegetation Index (EVI) from L8 measured 2 months before trappings ($t - 2$). Indeed, even if only EVI could be selected as the best predictor, most univariate models in Table 2 included L8 indices, and especially those measured at $t - 2$. Four S2 indices were included in this top 10 ranking, and three of them included the red edge band 5 and were

recorded at t_0. They are, however, distant in DIC terms from the resulting best predictor, i.e., for total mice count the only index that shows statistical support according to DIC values is L8 EVI_{t-2}.

To assess the effects of different spatial resolutions, we compared models including indices that are common to both S2 and L8 satellites estimated at t_0, $t - 1$ and $t - 2$. These results are presented in Table 3. We observed that S2 indices are only consistently better than those of L8 when we considered those taken simultaneously to mice trappings. Indeed, the lowest DIC in this comparison was achieved by the S2 Normalized Difference Water Index (NDWI). When comparing models with indices recorded at $t - 1$ and $t - 2$, L8 indices had a much lower DIC than S2 indices in the majority of cases. Notably, again NDWI, but from L8, was the best mice abundance predictor from the indices measured at $t - 1$ (Table 3).

Considering only indices that are exclusive to S2, the best models were those including the first and third red-edge bands (band 5 and 7, respectively) (Table 4) such as the NDVI at t_0 and the chlorophyll index (Clre) measured at $t - 1$ and $t - 2$. For t_0, the NDVI estimated with band 5 and the narrow NIR (band 8A) showed almost the same DIC value as the NDVI estimated with band 5 and 8.

When we compared univariate models for *A. azarae* and *C. musculinus*, we observed that the distribution of both species was better predicted (lowest DIC values) by indices obtained from S2 data (Table 5). The best index explaining *A. azarae's* distribution was $NDVI_{t-1}$ estimated with the second red edge band (band 6). Furthermore, this same index obtained at $t - 2$, the $NDVI_{t-1}$ estimated with the red edge band 7 and the Modified Simple Ratio red edge (MSRre) also showed statistical support according to the ΔDIC values. The index with the lowest DIC for *C. musculinus'* distribution models was $NDVI_{t-1}$ estimated with the red edge band 7. Notably, most models for this rodent species show ΔDIC < 2 (Table 5). Therefore it is difficult to identify a few meaningful indices. Tables comparing all S2 and L8 indices plus S2 specific indices separately for *A. azarae* and *C. musculinus* can be found in the Supplementary Material.

When splitting S2 and L8 indices at t_0, $t - 1$ and $t - 2$, we observed that only for some indices the difference in DIC values was higher than 2. In most cases this difference favoured S2 derived indices for predicting the distribution of the two most abundant rodent species (See Tables 1 and 3 in the Supplementary Material). NDVI and EVI derived from S2 satellite appeared repeatedly as good predictors at t_0 and $t - 1$ for both *A. azarae* and *C. musculinus*, as well as NDWI derived from L8. The $MNDWI_{t-2}$ derived from S2 was better than that of L8 for both mice species. Among the indices exclusive to S2, the best predictor of *A. azarae's* and *C. musculinus'* distribution was $NDVI_{t-1}$; for *A. azarae* it was estimated using red edge band 6 and for *C. musculinus* using red edge
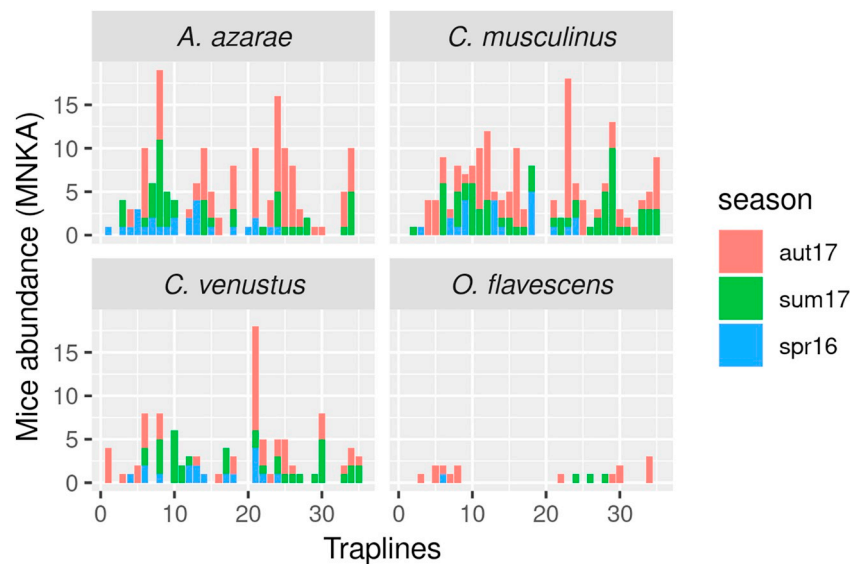
Fig. 3. Mice abundances as Minimum Number of Known Alive (MNKA) per species in each trapline and over the three sampling seasons (spr16: spring 2016, sum17: summer 2017 and aut17: autumn 2017) in the rural area of Chucul, central Argentina.

band 7. At $t − 2$, NDVI estimated with S2 band 6 appeared again as a good predictor for both species (Tables 2 and 4 in the Supplementary Material).

Fig. 5 shows the non-linear plots depicting the relationship among mice counts and probability of occurrence with vegetation indices for the models with the lowest DIC values. Fig. 5a shows that mice counts decrease when EVI $_{t−2}$ is below $\approx$ 0.5–0.6 and then increase. The probability of occurrence of *A. azarae* decreases with NDVI(B6&B8) $_{t−1}$ as well as that of *C. musculinus* as a function of NDVI(B7&B8) $_{t−1}$. The plots for all fitted models are included in the Supplementary Material. Note for example, that the NDWI both from S2 and L8, estimated at t_0 and $t − 1$ shows a positive association with mice counts.

4. Discussion

The overall goal of this study was to explore the potential of S2 as compared to L8 to predict mice abundance and distribution in border habitats of central Argentina's agroecosystems. Visually, S2 is better than L8 for the identification and delineation of such narrow rodents habitats (Fig. 2) (Radoux et al., 2016). When ranking models to account for mice abundance, however, the best predictor was EVI $_{t−2}$ from L8 (Table 2). Moreover, in the comparisons among S2 and L8 common indices to predict mice abundance, the S2 advantage in terms of spatial resolution was only evident for indices obtained simultaneously to mice trappings (Table 3). On the contrary, S2 indices seemed more relevant for modeling the distribution of the most common rodent species (Table 5). Indeed, the NDVI estimated with red edge bands 6 and 7 showed the lowest DIC values in models predicting the distribution of *A. azarae* and *C. musculinus*, respectively (Table 5). The importance of S2 red-edge bands was already reported in other studies that used these bands to measure chlorophyll content (Delegido et al., 2011), estimate burn severity (Fernández-Manso et al., 2016), predict leaf nitrogen content (Ramoelo et al., 2015) and map croplands (Kalluri et al., 2007).

The relevance of vegetation for rodent populations is well known, as it can provide shelter, food, nesting opportunities, as well as protection from predators. Different studies in Argentinean agroecosystems have also tested this relationship both with remote sensing and field data (Andreo et al., 2009a, b; Gomez et al., 2018; Polop et al., 2008; Polop et al., 2012; Simone et al., 2010; Simone et al., 2012). Our results pointed to EVI $_{t−2}$ derived from L8 as the best predictor (ΔDIC $<$ 2) of mice abundance. Even if EVI is generally known to correct for background and atmosphere noises (Gao et al., 2000; Huete et al., 1985),

this result does not fully support our initial hypothesis that S2 enhanced spatial resolution would perform better. Instead, it suggests that there must be some context environmental information relevant for mice abundances that is better captured by a 30 m side pixel rather than by a 10 m one. S2 indices, however, performed better than those derived from L8 for mice abundance models at t_0. This implies that if only simultaneous remote sensing data are available, then S2 is the best choice.

Sentinel-2 enhanced spatial and spectral resolution seemed to pay off for predicting *A. azarae* and *C. musculinus* distribution (Table 5). Indeed, the best predictors were derived from S2 data and included red edge and narrow NIR bands. We could infer from this that vegetation health and quality (as recorded by red edge NDVI) is a better determinant of mice distribution than of mice abundance. In this sense, *A. azarae* is known to prefer highly covered areas, and sexually active females select areas with great amounts of green cover (Bilenca and Kravetz, 1998; Ellis et al., 1997). Meanwhile, *C. musculinus* is a more opportunistic species and more tolerant to environmental changes (Busch et al., 2000; Mills et al., 1991). Both species displayed a negative association with red-edge NDVI$_{t−1}$, implying that higher vegetation cover/quality would yield lower presence probability in the next month. This might be consistent with the opportunistic nature of *C. musculinus* that is commonly found in crop fields (Mills et al., 1991) and also with the fact that *A. azarae* is a dominant competitor in borders, relegating the former to habitats of less quality within borders (Busch and Kravetz, 1992). For *A. azarae*, we would have expected a positive relation with NDVI as observed in seasonal and inter-annual studies (Andreo et al., 2009a, b). It has been observed, however, that *A. azarae* increases the use of cropfields during late spring and summer when they offer better cover and more food than borders (Bilenca and Kravetz, 1998). After the harvest, *A. azarae* returns to border habitats which quality is not so high but still better than cropfields (Cavia et al., 2005; Hodara and Busch, 2006). This differential use of borders and cropfields might explain the negative relation of *A. azarae* and red edge NDVI. In any case, a better comprehension of the red edge NDVI range of values with regards to field conditions, as well as the intra-seasonal relation to plant cover, would be needed.

The association of time lagged vegetation indices with mice abundances was already observed by (Andreo et al., 2009a, b) for *A. azarae*. This lagged response of mice abundances to their environment is generally expected given that rodent populations need to go through certain processes to respond to environmental changes. For instance, it
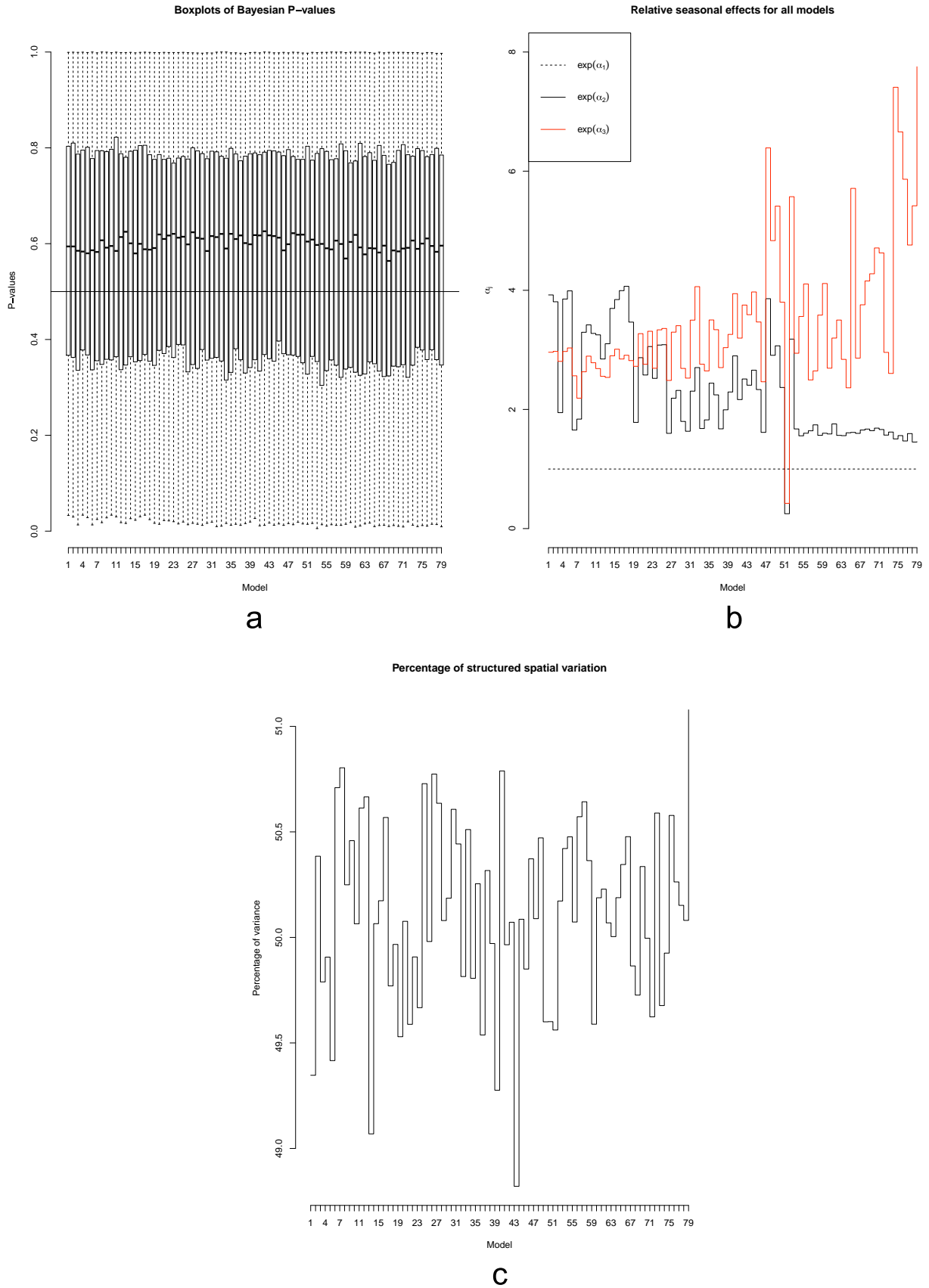
Boxplots of Bayesian P–values

Relative seasonal effects for all models

Percentage of structured spatial variation

Fig. 4. Adequacy assessment of models for mice abundance. (a). Bayesian *p*-values based on posterior probability distribution; (b). Relative seasonal effects for all models where spring (s0) is taken as reference; (c). Percentage of structured spatial variation across models. Models 1 to 26 correspond to t_0 indices, 27–53 to $t − 1$ indices and 54 to 80, $t − 2$.

Table 2
Ranking of the first 10 univariate models for total rodent counts in border habitats of agroecosystems of central Argentina (spring 2016-autumn 2017) sorted by Δ DIC values. Abbreviations: EVI-Enhanced Vegetation index; NDVI-Normalized Difference Vegetation Index; DVI-Difference Vegetation Index; NDWI-Normalized Difference Water Index; CLre-Chlorophyll Index red edge; GNDVI-Green Normalized Vegetation Index; t_0-simultaneous to the sampling date; $t-1$ and $t-2$-one and two months before the sampling date, respectively.

Index	Satellite	DIC	Δ DIC
EVI $_{t-2}$	L8	481.45	0.00
NDVI $_{t-2}$	L8	485.98	4.53
DVI $_{t-2}$	L8	487.66	6.22
NDWI $_{t-2}$	L8	493.40	11.95
Clre $_{t-2}$	S2	495.89	14.45
NDWI $_{t-1}$	L8	498.10	16.65
NDWI $_{t0}$	S2	499.22	17.77
GNDVI $_{t-2}$	L8	500.21	18.77
NDVI $_{t0}$ (B5&B8)	S2	500.86	19.41
NDVI $_{t0}$ (B5&B8A)	S2	500.95	19.51

Table 3
Comparison of univariate models for total rodent counts and S2 and L8 indices in border habitats of agroecosystems of central Argentina (spring 2016-autumn 2017).

Index	t_0		$t-1$		$t-2$	
	DIC (S2)	DIC (L8)	DIC (S2)	DIC (L8)	DIC (S2)	DIC (L8)
NDVI	501.97	511.27	514.72	502.44	506.33	485.98
EVI	505.78	510.79	510.70	504.65	501.81	**481.45**
GNDVI	502.10	508.11	510.44	501.58	511.64	500.21
DVI	507.21	511.30	510.17	513.78	503.70	487.66
SR	507.41	510.70	514.53	506.16	513.53	514.25
NDWI	**499.22**	507.68	510.63	**498.10**	510.54	493.40
MNDWI	515.91	517.90	512.05	512.12	516.44	507.10

Abbreviations: NDVI-Normalized Difference Vegetation Index; EVI-Enhanced Vegetation index; GNDVI-Green Normalized Vegetation Index; SR-Simple Ratio; DVI-Difference Vegetation Index; NDWI-Normalized Difference Water Index; MNDWI-Modified Normalized Difference Water Index; t_0-simultaneous to the sampling date; $t-1$ and $t-2$-one and two months before the sampling date, respectively.
Lowest DIC values per time lag are marked in bold for easier identification.

Table 4
Comparison of univariate models for total mice counts and S2 specific vegetation indices in border habitats of agroecosystems of central Argentina (spring 2016-autumn 2017).

S2 index	t_0	$t-1$	$t-2$
	DIC	DIC	DIC
NDVI (B5&B8)	**500.86**	515.85	507.60
NDVI (B6&B8)	505.91	512.75	515.64
NDVI (B7&B8)	nc	516.54	509.05
NDVI (B4&B8A)	502.72	511.68	511.55
NDVI (B5&B8A)	**500.95**	512.52	508.41
NDVI (B6&B8A)	516.20	514.20	517.25
NDVI (B7&B8A)	515.95	515.80	510.88
PSRI	506.90	514.66	504.34
Clre	505.22	**507.54**	**495.89**
MSRre	505.79	514.92	509.77
MSRren	503.86	509.39	513.71
NDre1	501.89	515.23	503.92
NDre2	502.73	514.34	508.28

Abbreviations: NDVI-Normalized Difference Vegetation Index; PSRI-Plant Senescence Reflectance Index; Clre-Chlorophyll Index red edge; MSRre-Modified Simple Ratio red-edge; MSRren-Modified Simple Ratio red-edge narrow; NDre1-Normalized Difference red-edge 1; NDre2-Normalized Difference red-edge 2; t_0-simultaneous to the sampling date; $t-1$ and $t-2$-one and two months before the sampling date, respectively; nc-no convergence. Lowest DIC values per time lag are marked in bold for easier identification.

takes ≈ 25 days of pregnancy plus at least other ≈ 40 days until sexual maturity (Mills et al., 1992). Therefore, 2 months of delay in the response as suggested by the best univariate models would mean that the effects of changes in vegetation cover in February, for example, will be visible in April (early autumn in the Southern hemisphere) mice abundances. One might hypothesize that a higher value of the vegetation index corresponds to higher mice abundances as observed when using linear models (Andreo et al., 2009c). The use of non-linear models, however, allows to uncover other types of relations (Fig. 5 and Supplementary Material). Indeed, the association of mice abundance with EVI$_{t-2}$ (Fig. 5a) shows that up to ≈ 0.5, mice abundances seem to decrease. This may be reflecting low EVI values in late March–April due to harvest or early frosts when abundances are still increasing to reach the annual peak by May–June (Andreo et al., 2009a, b; Simone et al., 2012). It was out of the scope of this study to test further time lags. Our results so far are consistent with previous studies using remotely sensed vegetation indices to predict mice abundances in agroecosystems (Andreo et al., 2009a,b).

Advantages of S2 increased spectral resolution for ecological applications involving vegetation and animals such as rodents have been proven in our study especially for mice distribution. More data would be necessary to test these indices as predictors of abundance on a per species basis. Unfortunately, however, S2 lacks thermal band and therefore it cannot be used to derive land surface temperature which is an important variable for identifying and monitoring numerous pathogens and insect vectors (Flood, 2017). Moreover, since S2 is a relatively new Earth Observation (EO) mission, applications requiring historical data will need to refer to Landsat or other EO records. In the perspective of a combined S2 and L8 use, there are some differences to be considered. On the one hand, previous studies have reported a misalignment of several pixels between L8 and S2 (Novelli et al., 2016). These misalignments are relevant when mapping the habitats of different disease hosts and vectors, or placing traplines in roadsides as in the present study. Therefore, images coming from the two sensors need to be manually co-registered (See Table 1). On the other hand, careful attention is required in the selection of the NIR bands used to compute vegetation indices, since the NDVI values computed using S2 band 8 proved to be lower than the L8 NDVI values (Mandanici and Bitelli, 2016). The plot presented in Fig. 6 depicts the time series of average NDVI and EVI per trapline as estimated by the data of each sensor plus a locally weighted smoothing line (LOESS). This difference might be relevant if data from the two satellites must be combined in a single time series (Steven et al., 2003; van Leeuwen et al., 2006). Previous studies suggested that S2 band 8A (narrow NIR at 20 m of spatial resolution) would be the best choice when combining images acquired by these two platforms since this band is spectrally more similar to the L8 NIR band (Zhang et al., 2018). In order to take advantage of the 10 m resolution of S2 band 8 (wider NIR) and use this data along with L8 data, the differences in the estimates of the biophysical variables by adjusting the reflectance values of the two sensors (Mandanici and Bitelli, 2016). Nonetheless, the discrepancy observed for NDVI seems to not affect EVI in our study area. Therefore, EVI might be a good candidate to build combined time series of L8 and S2 data.

Despite the above-mentioned challenges, S2 has opened new opportunities for ecological applications by allowing detailed mapping of

Table 5

Ranking of the first 15 univariate models for *A. azarae* and *C. musculinus*' distribution in border habitats of agroecosystems of central Argentina (spring 2016-autumn 2017) sorted by ΔDIC values. Abbreviations: GNDVI-Green Normalized Difference Vegetation Index; MSRen-Modified Simple Ratio red-edge narrow; NDre2-Normalized Difference red-edge 2; Clre-Chlorophyll Index red edge; EVI-Enhanced Vegetation index; DVI-Difference Vegetation Index; PSRI-Plant Senescence Reflectance Index; $t-1$ and $t-2$-one and two months before the sampling date, respectively.

Index	*A. azarae*			Index	*C. musculinus*		
	Satellite	DIC	Δ DIC		Satellite	DIC	Δ DIC
$NDVI_{t-1}$ (B6&B8)	S2	140.74	0.00	$NDVI_{t-1}$ (B7&B8)	S2	141.46	0.00
$NDVI_{t-2}$ (B6&B8)	S2	142.08	1.34	$MNDWI_{t-2}$	S2	141.75	0.30
$NDVI_{t-1}$ (B7&B8)	S2	142.64	1.90	$PSRI_{t-1}$	S2	142.51	1.05
MSRre	S2	142.64	1.90	EVI	S2	142.83	1.38
$MNDWI_{t-2}$	S2	143.02	2.28	NDre2	S2	142.86	1.41
PSRI	S2	143.21	2.47	$NDVI_{t-1}$ (B4&B8)	S2	142.98	1.53
$NDre1_{t-2}$	S2	143.28	2.54	NDVI (B4&B8A)	S2	143.12	1.67
NDVI (B5&B8)	S2	143.32	2.59	$NDVI_{t-2}$ (B6&B8)	S2	143.15	1.69
$NDW_{t-1}I$	L8	143.37	2.64	$PSRI_{t-2}$	S2	143.25	1.79
$NDVI_{t-2}$ (B5&B8)	S2	143.55	2.81	Clre	S2	143.26	1.81
$NDVI_{t-2}$ (B4&B8A)	S2	143.81	3.08	$NDVI_{t-2}$ (B5&B8A)	S2	143.31	1.85
SR_{t-1}	S2	143.88	3.14	SR_{t-1}	S2	143.41	1.96
EVI	S2	144.03	3.29	$NDVI_{t-2}$ (B7&B8)	S2	143.58	2.12
NDre2	S2	144.24	3.51	$NDVI_{t-1}$	L8	143.72	2.26

habitats (Shoko and Mutanga, 2017; Traganos and Reinartz, 2018) and environmental variables. Additionally, the 5 ays revisit time of S2 offers an unprecedented possibility to monitor environmental variables and their dynamics in an operational context and completely free of charge. Our findings are relevant for ecologists and other researchers using remote sensing data to predict animal distribution and abundances, especially animals involved in zoonotic diseases cycles. Moreover, some of the indices that appeared significant were those obtained 1 and 2 months before the trappings, which would allow for example, the use of S2 together with L8 in operative monitoring systems for early warning (Porcasi et al., 2012). There are already some efforts aimed at providing harmonized Landsat/Sentinel data (Helder et al., 2018) from which many applications will benefit.

5. Conclusions

We explored the spatial and spectral potential of S2 data for predicting mice abundances and distribution. S2 derived indices outperformed those from L8 only when indices were computed simultaneously to trappings in the case of abundances and, for distribution models. This indicates that an enhanced spatial resolution not always yields better predictions. We further showed the relevance of the narrow NIR and red-edge bands-based vegetation indices to predict mice distribution in an agroecosystems of central Argentina. The findings of this study can be used as guidelines when selecting the sensors and vegetation variables to be included in more complex models aimed at predicting the distribution and risk of various vector-borne diseases, and especially rodents in other agricultural landscapes.
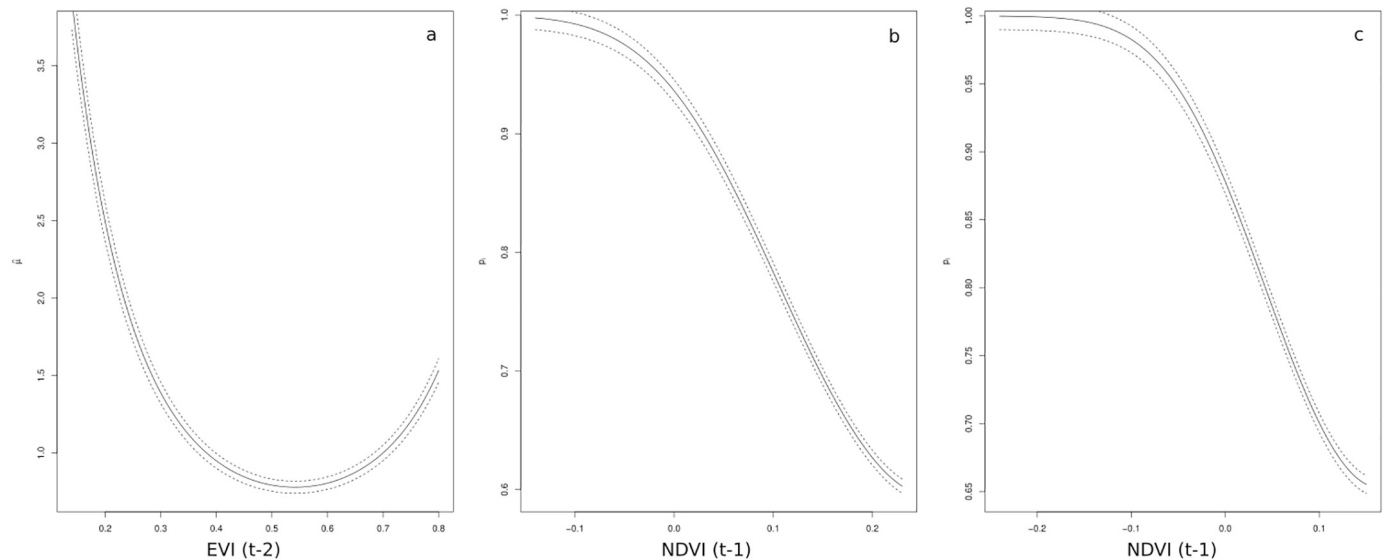

Fig. 5. Non-linear curves for models with the lowest DIC. (a). Mice counts ($\hat{\mu}$) vs EVI_{t-2}; (b). *A. azarae* presence probability (ρ_i) vs NDVI(B6&B8) $_{t-1}$; (c). *C. musculinus* presence probability (ρ_i) vs NDVI(B7&B8) $_{t-1}$.
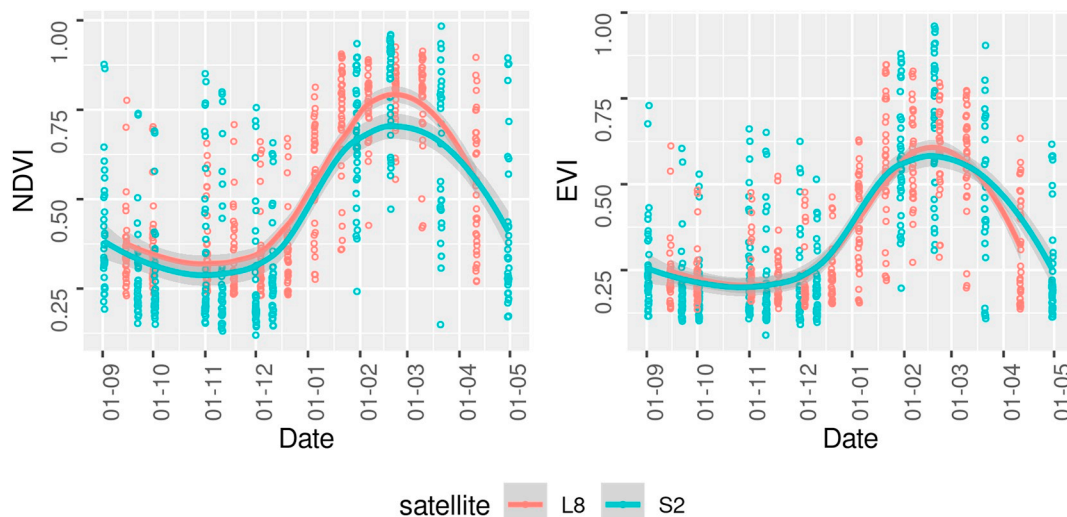
Fig. 6. Time series plot of S2 and L8 average NDVI and EVI for the period September 2016–April 2017. A total of 11 S2 and 12 L8 scenes were processed and the values of NDVI and EVI were extracted.

Acknowledgements

Appendix

Table 6
Description of indices derived from Sentinel-2 (S2) and Landsat 8 (L8) imagery.

Acronym	Description	Equation	S2	L8	Reference
NDVI	Normalized Difference Vegetation Index	$NDVI = \frac{NIR - Red}{NIR + Red}$	x	x	(Merzlyak et al., 1999)
EVI	Enhanced Vegetation index	$EVI = G*\frac{NIR - Red}{NIR + C1*Red - C2*Blue + L}$	x	x	
GNDVI	Green Normalized Vegetation index	$GNDVI = \frac{Green - Red}{Green + Red}$	x	x	
SR	Simple Ratio	$SR = \frac{NIR}{Red}$	x	x	
DVI	Difference Vegetation Index	$DVI = NIR - Red$	x	x	
NDVI (B8 & B5)	Normalized Difference Vegetation Index with red edge 1	$NDVI = \frac{NIR - Red\ Edge^*}{NIR + Red\ Edge^*}$	x		(Gitelson et al., 2003)
NDVI (B8 & B6)	Normalized Difference Vegetation Index with red edge 2	$NDVI = \frac{NIR^a - Red\ Edge^{**}}{NIR + Red\ Edge^{**}}$	x		(Fernández-Manso et al., 2016)
NDVI (B8 & B7)	Normalized Difference Vegetation Index with red edge 3	$NDVI = \frac{NIR^a - Red\ Edge^{***}}{NIR + Red\ Edge^{***}}$	x		(Fernández-Manso et al., 2016)
NDVI (B8A & B5)	Normalized Difference Vegetation Index with red edge 1 narrow	$NDVI = \frac{NIR^a - Red\ Edge^*}{NIR^a + Red\ Edge^*}$	x		(Fernández-Manso et al., 2016)
NDVI (B8A & B6)	Normalized Difference Vegetation Index with red edge 2 narrow	$NDVI = \frac{NIR^a - Red\ Edge^{**}}{NIR^a + Red\ Edge^{**}}$	x		(Fernández-Manso et al., 2016)
NDVI (B8A & B7)	Normalized Difference Vegetation Index with red edge 3 narrow	$NDVI = \frac{NIR^a - Red\ Edge^{***}}{NIR^a + Red\ Edge^{***}}$	x		(Fernández-Manso et al., 2016)
PSRI	Plant Senescence Reflectance Index	$PSRI = \frac{NIR - Green}{Red\ Edge^*}$	x		(Barnes et al., 2000)
Clre	Chlorophyll Index red edge	$CLre = \frac{Red\ Edge^{***}}{Red\ Edge^*} - 1$	x		(Chen, 1996)
NDre1	Normalized Difference red-edge 1	$NDre1 = \frac{Red\ Edge^{**} - Red\ Edge^*}{Red\ Edge^{**} + Red\ Edge^*}$	x		(Gitelson et al., 2003)
NDre2	Normalized Difference red-edge 2	$NDre2 = \frac{Red\ Edge^{***} - Red\ Edge^*}{Red\ Edge^{***} + Red\ Edge^*}$	x		(Barnes et al., 2000)
MSRre	Modified Simple Ratio red-edge	$MSRre = \frac{\frac{NIR}{Red\ Edge^*} - 1}{\sqrt{\frac{NIR}{Red\ Edge^*}} - 1}$	x		(Chen, 1996)
MSRren	Modified Simple Ratio red-edge narrow	$MSRren = \frac{\frac{NIR^a}{Red\ Edge^*} - 1}{\sqrt{\frac{NIR^a}{Red\ Edge^*}} - 1}$	x		(Fernández-Manso et al., 2016)
NDWI	Normalized Difference Water Index	$NDWI = \frac{Green - NIR}{Green + NIR}$	x	x	(McFeeters, 1996)
MNDWI	Modified Normalized Difference Water Index	$MNDWI = \frac{Green - SWIR^b}{Green + SWIR^b}$	x	x	(Xu, 2006)

References: *a*: narrow NIR (band 8A); *b*: SWIR (band 11); *: Red-edge 1 (band 5); **: Red-edge 2 (band 6); ***: Red-edge 3 (band 7).

References

Andreo, V., Lima, M., Provensal, C., Priotto, J., Polop, J., 2009a. Population dynamics of two rodent species in agro-ecosystems of central Argentina: intra-specific competition, land-use, and climate effects. Popul. Ecol. 51, 297–306. https://doi.org/10.1007/s10144-008-0123-3. http://www.springerlink.com/index/10.1007/s10144-008-0123-3.

Andreo, V., Provensal, C., Scavuzzo, M., Lamfri, M., Polop, J., 2009b. Environmental factors and population fluctuations of *Akodon azarae* (Muridae: Sigmodontinae) in Central Argentina. Aust. Ecol. 132–142. https://doi.org/10.1111/j.1442-9993.2008.01889.x.

Andreo, V., Glass, G., Shields, T., Provensal, C., Polop, J., 2011. Modeling potential distribution of *Oligoryzomys longicaudatus*, the Andes virus (genus: Hantavirus) reservoir, in Argentina. EcoHealth 8, 332–348.

Andreo, V., Neteler, M., Rocchini, D., Provensal, C., Levis, S., Porcasi, X., Rizzoli, A., Lanfri, M., Scavuzzo, M., Pini, N., Enria, D., Polop, J., 2014. Estimating hantavirus risk in southern Argentina: a GIS-based approach combining human cases and host distribution. Viruses 6, 201–222. https://doi.org/10.3390/v6010201.

Barnes, E.M., Clarke, T.R., Richards, S.E., Colaizzi, P.D., Haberland, J., Kostrzewski, M., Waller, P., Choi, C., Riley, E., Thompson, T., 2000. Coincident detection of crop water stress, Nitrogen status and canopy density using ground based multispectral data. In: Proceedings of the Fifth International Conference on Precision Agriculture, ASA, CSSA, and SSSA, Madison, WI, Bloomington, MN, USA, pp. 1–15.

Beck, L.R., Lobitz, B.M., Wood, B.L., 2000. Remote sensing and human health: new sensors and new opportunities. Emerg. Infect. Dis. 6, 217.

Bilenca, D.N., Kravetz, F.O., 1998. Seasonal variations in microhabitat use and feeding habits of the pampas mouse *Akodon azarae* in agroecosystem of central Argentina. Acta Theriol. 43 (2), 195–203.

Busch, M., Kravetz, F., 1992. Competitive interactions among rodents (*Akodon azarae*, *Calomys laucha*, *Calomys musculinus* and *Oligoryzomys flavescens*) in a two-habitat system. ii. effect of species removal. Mammalia 56, 541–553.

Busch, M., Miño, M.H., Dadon, J.R., Hodara, K., 2000. Habitat selection by *Calomys musculinus* (Muridae, Sigmodontinae) in crop areas of the pampean region, Argentina. Ecol. Aust. 15–26.

G. Calderón, F. Piacenza, J. García, J. J. Polop, D. Enría, S. Levis, Circulación del virus Latino (Familia Arenaviridae, Género Arenavirus) en la región central de Argentina, Rev. Argent. Microbiol. 1 (12).

Carroll, M., Townshend, J.R., DiMiceli, C.M., Noojipady, P., Sohlberg, R.A., 2009. A new global raster water mask at 250 m resolution. Int. J. Digital Earth 2 (4), 291–308.

Cavia, R., Villafane, I., Cittadino, E., Bilenca, D., Mino, M., Busch, M., 2005. Effects of cereal harvest on abundance and spatial distribution of the rodent in central argentina. 107 (1), 95–99. https://doi.org/10.1016/j.agee.2004.09.011. http://linkinghub.elsevier.com/retrieve/pii/S0167880904002944.

J. M. Chen, Evaluation of vegetation indices and a modified simple ratio for boreal applications, Can. J. Remote. Sens. 22 (3) (1996) 229–242. doi:https://doi.org/10.1080/07038992.1996.10855178. URL https://doi.org/10.1080/07038992.1996.10855178.

Delegido, J., Verrelst, J., Alonso, L., Moreno, J., 2011. Evaluation of Sentinel-2 red-edge bands for empirical estimation of green LAI and chlorophyll content. Sensors 11 (7), 7063–7081.

Dörnhöfer, K., Göritz, A., Gege, P., Pflug, B., Oppelt, N., 2016. Water constituents and water depth retrieval from Sentinel-2A – a first evaluation in an oligotrophic lake. Remote Sens. 8, 941. https://doi.org/10.3390/rs8110941.

Ellis, B., Mills, J., Childs, J., Muzzini, M., McKee, K., Enria, D., Glass, G., 1997. Structure and floristics of habitats associated with five rodent species in an agroecosystem in central Argentina. J. Zool. 243 (3), 437–460.

Fernández-Manso, A., Fernández-Manso, O., Quintano, C., 2016. Sentinel-2A red-edge spectral indices suitability for discriminating burn severity. Int. J. Appl. Earth Obs. Geoinf. 50, 170–175. https://doi.org/10.1016/j.jag.2016.03.005. http://www.sciencedirect.com/science/article/pii/S0303243416300368.

Flood, N., 2017. Comparing Sentinel-2A and Landsat 7 and 8 using surface reflectance over Australia. Remote Sens. 9 (7), 659.

Gao, X., Huete, A.R., Ni, W., Miura, T., 2000. Optical–biophysical relationships of vegetation spectra without background contamination. Remote Sens. Environ. 74 (3), 609–620.

Gitelson, A.A., Gritz, Y., Merzlyak, M.N., 2003. Relationships between leaf chlorophyll content and spectral reflectance and algorithms for non destructive chlorophyll assessment in higher plant leaves. J. Plant Physiol. 160 (3), 271–282.

Glass, G.E., Yates, T.L., Fine, J.B., Shields, T.M., Kendall, J.B., Hope, A.G., Parmenter, C.a., Peters, C.J., Ksiazek, T.G., Li, C.-S., Patz, J.a., Mills, J.N., 2002. Satellite imagery characterizes local animal reservoir populations of Sin Nombre virus in the southwestern United States. Proc. Natl. Acad. Sci. U. S. A. 99, 16817–16822. https://doi.org/10.1073/pnas.252617999.

Gomez, M.D., Goijman, A.P., Coda, J., Serafini, V., Priotto, J., 2018. Small mammal responses to farming practices in central Argentinian agroecosystems: the use of hierarchical occupancy models. Aust. Ecol. 43, 828–838. https://doi.org/10.1111/aec.12625. https://onlinelibrary.wiley.com/doi/abs/10.1111/aec.12625.

GRASS Development Team, 2018. Geographic Resources Analysis Support System (GRASS GIS) Software, Version 7.4, Open Source Geospatial Foundation. URL http://grass.osgeo.org.

Green, P., Yandell, B., 1985. Semi-parametric generalized linear models. In: Gilchrist, R., Francis, B., Whittaker, J. (Eds.), Generalized Linear Models. Springer, US, New York, pp. 44–55.

Hedley, J., Roelfsema, C., Koetz, B., Phinn, S., 2012. Capability of the Sentinel-2 mission for tropical coral reef mapping and coral bleaching detection. Remote Sens. Environ. 120, 145–155. https://doi.org/10.1016/j.rse.2011.06.028. http://www.sciencedirect.com/science/article/pii/S0034425712000715.

Helder, D., Markham, B., Morfitt, R., Storey, J., Barsi, J., Gascon, F., Clerc, S., LaFrance, B., Masek, J., Roy, D., Lewis, A., Pahlevan, N., 2018. Observations and recommendations for the calibration of landsat 8 OLI and sentinel 2 MSI for improved data interoperability. Remote Sens. 10 (9), 1340. https://doi.org/10.3390/rs10091340. http://www.mdpi.com/2072-4292/10/9/1340.

Hodara, K., Busch, M., 2006. Return to preferred habitats (edges) as a function of distance in *Akodon azarae* (Rodentia, Muridae) in cropfield-edge systems of central Argentina. J. Ethol. 24, 141–145.

Huete, A., Jackson, R., Post, D., 1985. Spectral response of a plant canopy with different soil backgrounds. Remote Sens. Environ. 17 (1), 37–53.

Immitzer, M., Vuolo, F., Atzberger, C., 2016. First experience with Sentinel-2 data for crop and tree species classifications in central Europe. Remote Sens. 8, 166. https://doi.org/10.3390/rs8030166.

Kalluri, S., Gilruth, P., Rogers, D., Szczur, M., 2007. Surveillance of arthropod vectorborne infectious diseases using remote sensing techniques: a review. PLoS Pathog. 3 (10), e116.

Levis, S., Morzunov, S.P., Rowe, J.E., Enria, D., Pini, N., Calderon, G., Sabattini, M., Jeor, S.C.St., 1998. Genetic diversity and epidemiology of hantaviruses in Argentina. J. Infect. Dis. 177 (3), 529–538.

Lunn, D., Jackson, C., Best, N., Thomas, A., Spiegelhalter, D., 2012. The BUGS Book: A Practical Introduction to Bayesian Analysis. Chapman and Hall/CRC.

O. E. Malahlela, J. M. Olwoch, C. Adjorlolo, Evaluating efficacy of landsat-derived environmental covariates for predicting malaria distribution in rural villages of Vhembe district, South Africa, EcoHealth 15 (1) (2018) 23–40. doi:https://doi.org/10.1007/s10393-017-1307-0. URL https://doi.org/10.1007/s10393-017-1307-0.

Mandanici, E., Bitelli, G., 2016. Preliminary comparison of Sentinel-2 and Landsat 8 imagery for a combined use. Remote Sens. 8 (12), 1014.

S. K. McFeeters, The use of the normalized difference water index (NDWI) in the delineation of open water features, Int. J. Remote Sens. 17 (7) (1996) 1425–1432. doi:https://doi.org/10.1080/01431169608948714. URL https://doi.org/10.1080/01431169608948714.

Meerburg, B.G., Singleton, G.R., Kijlstra, A., 2009. Rodent-borne diseases and their risks for public health. Crit. Rev. Microbiol. 35, 221–270. https://doi.org/10.1080/10408410902989837.

Merzlyak, M.N., Gitelson, A.A., Chivkunova, O.B., Rakitin, V.Y., 1999. Non-destructive optical detection of pigment changes during leaf senescence and fruit ripening. Physiol. Plant. 106 (1), 135–141.

Midekisa, A., Senay, G.B., Wimberly, M.C., 2014. Multisensor earth observations to characterize wetlands and malaria epidemiology in Ethiopia. Water Resour. Res. 50 (11), 8791–8806.

Mills, J.N., Childs, J.E., 1998. Ecologic studies of rodent reservoirs: their relevance for human health. Emerg. Infect. Dis. 4 (4), 529–537.

Mills, J.N., Ellis, B.A., McKee, K.T., Maiztegui, J.I., Childs, J.E., 1991. Habitat associations and relative densities of rodent populations in cultivated areas of central Argentina. J. Mammal. 72 (3), 470–479.

Mills, J.N., Ellis, B.A., McKee, K.T., Maiztegui, J.I., Childs, J.E., 1992. Reproductive characteristics of rodent assemblages in cultivated regions of central Argentina. J. Mammal. 73 (3), 515–526.

Muller-Wilm, U., Louis, J., Richter, R., Gascon, F., Niezette, M., 2013. Sentinel-2 level 2A prototype processor: architecture, algorithms and first results. In: Proceedings of the ESA Living Planet Symposium, Edinburgh, UK, pp. 9–13.

M. Neteler, D. Roiz, D. Rocchini, C. Castellani, A. Rizzoli, Terra and Aqua satellites track tiger mosquito invasion: modelling the potential distribution of *Aedes albopictus* in North-Eastern Italy, Int. J. Health Geogr. 10 (2011) 133–138. doi:https://doi.org/10.1186/1476-072x-10-49. URL https://doi.org/10.1186/1476-072X-10-49.

Ng, W.-T., Rima, P., Einzmann, K., Immitzer, M., Atzberger, C., Eckert, S., 2017. Assessing the potential of Sentinel-2 and Pléiades data for the detection of Prosopis and Vachellia spp. in Kenya. Remote Sens. 9 (1), 74. https://doi.org/10.3390/rs9010074. URL http://www.mdpi.com/2072-4292/9/1/74.

Novelli, A., Aguilar, M.A., Nemmaoui, A., Aguilar, F.J., Tarantino, E., 2016. Performance evaluation of object based greenhouse detection from Sentinel-2 MSI and Landsat 8 OLI data: a case study from AlmerÃa (Spain). Int. J. Appl. Earth Obs. Geoinf. 52, 403–411. https://doi.org/10.1016/j.jag.2016.07.011. http://www.sciencedirect.com/science/article/pii/S0303243416301180.

Ostfeld, R., Glass, G., Keesing, F., 2005. Spatial epidemiology: an emerging (or re-emerging) discipline. Trends Ecol. Evol. 20, 328–336. https://doi.org/10.1016/j.tree.2005.03.009.

Peckham, R., Sinha, R., 2017. Satellites and the new war on infection: tracking Ebola in West Africa. Geoforum 80, 24–38. https://doi.org/10.1016/j.geoforum.2017.01.001. URL www.sciencedirect.com/science/article/pii/S0016718517300015.

Polop, F., Provensal, C., Scavuzzo, M., Lamfri, M., Calderón, G., Polop, J., 2008. On the relationship between the environmental history and the epidemiological situation of Argentine Hemorrhagic Fever. Ecol. Res. 23, 217–225. https://doi.org/10.1007/s11284-007-0371-2.

Polop, F., Provensal, M.C., Priotto, J., Steinmann, A., Polop, J.J., 2012. Differential effects of climate, environment, and land use on two sympatric species of *Akodon*. Stud. Neotropical Fauna Environ. 47, 147–156. https://doi.org/10.1080/01650521.2012.736730.

Porcasi, X., Rotela, C.H., Introini, M.V., Frutos, N., Lanfri, S., Peralta, G., De Elia, E.A., Lanfri, M.A., Scavuzzo, C.M., 2012. An operative dengue risk stratification system in Argentina based on geospatial technology. Geospat. Health 6 (3), 31–42.

Radoux, J., Chomé, G., Jacques, D.C., Waldner, F., Bellemans, N., Matton, N., Lamarche,

C., d'Andrimont, R., Defourny, P., 2016. Sentinel-2's potential for sub-pixel landscape feature detection. Remote Sens. 8 (6), 488. https://doi.org/10.3390/rs8060488. URL http://www.mdpi.com/2072-4292/8/6/488.

A. Ramoelo, M. Cho, R. Mathieu, A. Skidmore, Potential of Sentinel-2 spectral configuration to assess rangeland quality., J. Appl. Remote. Sens. 9 (1) (2015) 094096–094096. doi:https://doi.org/10.1117/1.JRS.9.094096. URL https://doi.org/10.1117/1.JRS.9.094096.

Sabattini, M., Oro, J., Maiztegui, J., Fernandez, D., Costigiani, M., Diaz, G., 1970. Aislamiento de un arenovirus relacionado con el virus de la Coriomeningitis Linfocítica (LCM) a partir de un *Mus musculus* capturado en zona endémica de Fiebre Hemorrágica Argentina (FHA). Rev. Asoc. Argent. Microbiol. 2, 182.

Shoko, C., Mutanga, O., 2017. Examining the strength of the newly-launched sentinel 2 MSI sensor in detecting and discriminating subtle differences between c3 and c4 grass species. ISPRS J. Photogramm. Remote Sens. 129, 32–40. https://doi.org/10.1016/j.isprsjprs.2017.04.016. http://www.sciencedirect.com/science/article/pii/S0924271616306128.

Simone, I., Cagnacci, F., Provensal, C., Polop, J., 2010. Environmental determinants of the small mammal assemblage in an agroecosystem of Central Argentina: the role of *Calomys musculinus*. Mammalian Biology – Zeitschrift für Säugetierkunde 75, 496–509. https://doi.org/10.1016/j.mambio.2009.12.002.

Simone, I., Provensal, C., Polop, J., 2012. Habitat use by corn mice (*Calomys musculinus*) in cropfield borders of agricultural ecosystems in Argentina. Wildl. Res. 39, 112–122. https://doi.org/10.1071/WR11065.

Spiegelhalter, D.J., 2008. Understanding uncertainty. Ann. Family Med. 6 (3), 196–197.

Spiegelhalter, D.J., Best, N.G., Carlin, B.P., Van Der Linde, A., 2002. Bayesian measures of model complexity and fit. J. Roy. Stat. Soc.: Ser. B (Stat. Methodol.) 64 (4), 583–639.

Steven, M.D., Malthus, T.J., Baret, F., Xu, H., Chopping, M.J., 2003. Intercalibration of vegetation indices from different sensor systems. Remote Sens. Environ. 88 (4), 412–422. https://doi.org/10.1016/j.rse.2003.08.010. http://linkinghub.elsevier.com/retrieve/pii/S0034425703002256.

Traganos, D., Reinartz, P., 2018. Mapping mediterranean seagrasses with sentinel-2 imagery. Mar. Pollut. Bull. 134, 197–209. https://doi.org/10.1016/j.marpolbul.2017.06.075. http://www.sciencedirect.com/science/article/pii/S0025326X17305726.

van Leeuwen, W.J., Orr, B.J., Marsh, S.E., Herrmann, S.M., 2006. Multi-sensor NDVI data continuity: uncertainties and implications for vegetation monitoring applications. Remote Sens. Environ. 100 (1), 67–81. http://linkinghub.elsevier.com/retrieve/pii/S003442570500341X.

Verhegghen, A., Eva, H., Ceccherini, G., Achard, F., Gond, V., Gourlet-Fleury, S., Cerutti, P., 2016. The potential of Sentinel satellites for burnt area mapping and monitoring in the Congo Basin forests. Remote Sens. 8 (12), 986. URL http://www.mdpi.com/2072-4292/8/12/986.

Watson, D.C., Sargianou, M., Papa, A., Chra, P., Starakis, I., Panos, G., 2014. Epidemiology of hantavirus infections in humans: a comprehensive, global overview. Crit. Rev. Microbiol. 40, 261–272. https://doi.org/10.3109/1040841X.2013.783555.

H. Xu, Modification of normalised difference water index (NDWI) to enhance open water features in remotely sensed imagery, Int. J. Remote Sens. 27 (14) (2006) 3025–3033. doi:https://doi.org/10.1080/01431160600589179. URL https://doi.org/10.1080/01431160600589179.

Zhang, H.K., Roy, D.P., Yan, L., Li, Z., Huang, H., Vermote, E., Skakun, S., Roger, J.-C., 2018. Characterization of sentinel-2a and landsat-8 top of atmosphere, surface, and nadir brdf adjusted reflectance and ndvi differences. Remote Sens. Environ. https://doi.org/10.1016/j.rse.2018.04.031. in press. http://www.sciencedirect.com/science/article/pii/S0034425718301883.

Zheng, H., Du, P., Chen, J., Xia, J., Li, E., Xu, Z., Li, X., Yokoya, N., 2017. Performance evaluation of downscaling Sentinel-2 imagery for land use and land cover classification by spectral-spatial features. Remote Sens. 9 (12), 1274. https://doi.org/10.3390/rs9121274. http://www.mdpi.com/2072-4292/9/12/1274.